MULTISCALE HOMOGENIZATION AND ANALYSIS OF ANISOTROPIC ASSEMBLIES AS COSSERAT CONTINUA

Nicholas Fantuzzi,[1,*] Farui Shi,[1,2,3] Marco Colatosti,[4] & Raimondo Luciano[5]

[1]*DICAM Department, University of Bologna, Viale del Risorgimento 2, 40136, Bologna, Italy.*

[2]*State Key Laboratory of Coal Mine Disaster Dynamics and Control, Chongqing University, No.174 Shazhengjie, Shapingba, Chongqing, 400044, China.*

[3]*School of Resources and Safety Engineering, Chongqing University, No.174 Shazhengjie, Shapingba, Chongqing, 400044, China.*

[4]*DISG Department, Sapienza University of Rome, Via A. Gramsci, 53, 00197, Roma, Italy*

[5]*Engineering Department, Parthenope University, Centro Direzionale (Isola C4), 80133, Napoli, Italy*

*Address all correspondence to: Nicholas Fantuzzi, DICAM Department, University of Bologna, Viale del Risorgimento 2, 40136, Bologna, Italy., E-mail: nicholas.fantuzzi@unibo.it

This work proposes a multiscale analysis of nanocomposites made of hexagonal assemblies. The present nanomaterial is made of irregular concave hexagonal shaped assemblies interacting with elastic interfaces. The homogenization of such irregular units results to have anisotropic constitutive properties by applying a homogenization method. The validity of the present homogenization and modeling is verified by comparing the continuum Cosserat model with a discrete model made of physical particles and elastic interfaces. Parametric investigation is also proposed by varying the geometric properties of the nanoparticles by showing the dynamic character of these materials by considering both Cosserat and Cauchy contiuum models.

KEY WORDS: *cosserat continua, anisotropic media, relative rotation, composites/masonry, finite element method*

1543–1649/17/$35.00

1. INTRODUCTION

It is well known that multiscale methods have been introduced when continuum mechanics was developed. Since mechanical properties introduced in the latter should have been determined for the solution of the formulated mathematical problem. The most compelling multiscale approaches are the ones that provide macroscale relations by taking into consideration the underlying microscale. This connection is often provided by equivalence criteria (Trovalusci, 2014). Since originally elastic continua were modeled as interaction of particles/molecules depending on their mutual distance, an approach based on mechanics was able to predict the macroscopic constitutive behavior using microscopic laws for systems of particles/molecules (also known as central-force scheme). The latter provided the basis of the well-known Cauchy model of the elastic body where all particles/molecules are in contact in pairs.

The original definition provided by Cauchy has been extended by Voigt by introducing a continuum made of oriented rigid particles that interact among forces and couples. He was able to demonstrate that Navier-Cauchy molecular theory was not correct due to the assumption of a central-force scheme, since orientation of the particles was not taken into consideration (Trovalusci, 2014). The one that was able to overcome the limitations of molecular approaches in elasticity was Poincaré (Trovalusci, 2014). Poincaré proposed a lattice model described by potential energy function of point-like molecules which were able not only to interact in pairs, but also to give a multibody potential description (Mariano and Trovalusci, 1999). It should be underlined that molecular mechanical theories were based on the discrete nature of matter. The same was applied also in thermodynamics (Cimmelli et al., 2013; Li and Ostoja-Starzewski, 2011; Makowski and Stumpf, 2001)), electromagnetics and quantum mechanics too (Blanc et al., 2002; Curtin and Miller, 2003).

As aforementioned, the mechanical properties of materials need a microstructure description in order to be accurately predicted and carried out by homogenization procedures (Budiansky, 1965; Nemat-Nasser et al., 1996). In particular, several length scales are often required, thus, discrete-continuous approaches are encountering a renewal. It is worth to mention that coarse–graining homogenizations exploit an explicit link between the fine and coarse scales, moreover, they keep memory of the microstructural origin of deformation mechanisms which is especially needed in novel custom-made materials (Sadowski et al., 2014).

Homogeneous deformations are considered in both Voigt's and Poincaré's models (in other words local actions are considered) and local angular potential are added to the local actions. At this stage, if no other constraint is applied the homogenized continua would exhibit its dependency on material length scales (Maugin, 2016). These models can be termed as 'implicit' non–local continua as described by Mindlin (1964) and Trovalusci (2014). On the contrary if not homogeneous deformations are taken into account the equivalent continua would be classified as 'explicit'

non–local media such as by Eringen (1972) and Tuna et al. (2019). The aforementioned approach of Voigt related to coarse-graining approach can be used in several composite material configurations such as fiber-reinforced materials, microcracked solids (Greco et al., 2016a; Jain and Ghosh, 2009; Nguyen et al., 2012), voids and gaps (Pingaro et al., 2019a) and dilatant materials (Shi et al., 2021). De Borst (1991) and Sluys et al. (1993) showed the advantages of materials with microstructure when localization and discontinuities are introduced in the continuum.

As it has been demonstrated also by Kunin (2012), the description of materials with an internal microstructure (e.g. materials made of constituents of significant size) must consider nonlocal modelling. The latter (also known as microcontinua or complex continua as shown by Sadowski and Trovalusci (2014)) defines any continuum that keeps memory of the internal microstructure by means of internal material lengths which often represent the distance between particles in a lattice, grain or cell size, etc. as also discussed by Shaat et al. (2020). Nonlocal continua are known to have dispersion properties which represent a dependency between wave–velocities and wave–length/frequency (Cermelli and Pastrone, 2001; Kumar et al., 2008; Mondal et al., 2021; Oliveri and Speciale, 2008). Classical continuum modelling (also known as Grade 1 (Trovalusci, 2014) do not have the aforementioned properties.

It is noted that 'implicit' (weak) and 'explicit' (strong) nonlocal models both include internal length parameters in their mathematical formulation and their equations show dispersion properties (Eringen, 1983; Kröner, 1963)) and more recently by (Tuna et al., 2020; Tuna and Trovalusci, 2020). All these models are described by an extended virtual power framework, with classical and non-classical primary variables coupled with dual standard and/or non–standard fields (Trovalusci, 2014).

Explicit nonlocal models are higher grade theories where the equations of motions contain derivatives in space or time of the standard primal field (macrovelocity) of order different than the second as in the works by Bassani et al. (2001); De Borst and Mühlhaus (1992); Mühlhaus and Aifantis (1991); Needleman (1988) among others. In this regard, it is worth to cite also the contributions by Bažant et al. (1984); Pijaudier-Cabot and Bazant (1987). Regarding the other set of equations of motion that contain non–standard primal fields can be divided into two further classes. Firstly, the ones that can be derived from the standard frame invariance axioms, as in the classical case (Green and Rivlin, 1997; Podio-Guidugli and Vianello, 2010). Secondly, additional degrees of freedom are considered which contain non standard primal fields and – eventually – their derivatives. The latter set of equations are derived using a different axiomatic framework as discussed by Gurtin and Podio-Guidugli (1992); Yavari and Marsden (2009)

The modern concept of material theories with additional degrees of freedom has been provided in the 50s by Ericksen and Truesdell (1957); Mindlin (2021), however, the seminal work by Mindlin (1964) shed the light on continua with additional degrees of freedom which were able to keep memory of the material microstructure. In order

to provide such information microstructure is identified by a unit cell (also known as reference volume element) as a portion of polycrystal or granular material as in Gerolymatou (2014); Luding (2005); Settimi et al. (2019). Cosserat theory became very popular since the 70s due to the introduction of composite materials in most engineering practices since most application have geometric and/or load discontinuities, both conditions wherein Cosserat models work better than classical continuum (Cowin, 1970; Luciano and Barbero, 1995). In the same context the multiscale homogenization of random composites is worth to be mentioned for its applicability (Luciano and Willis, 2000, 2003, 2005, 2006; Pingaro et al., 2019b).

The present work lays in the field of molecular-multifield models for composite materials. The procedure here considered takes the advantage of an enriched macroscopic multifield model which is able to consider the description of the material at the microscopic level (Trovalusci and Masiani, 1999). The material is considered here as a set of rigid particles with a deformable matrix and their interaction depends only on their assemblage where also particle orientation is taken into consideration. Material porosity can be also considered since it has an important role. It has been demonstrated in the recent literature that the present model is able to analyze fibre-reinforced ceramics, porous ceramic composites or metal-ceramic composites but also geomaterials or jointed rocks (Adhikary and Dyskin, 1997; Adhikary et al., 1999; Li et al., 2009; Lu et al., 2020)) and masonry (Greco et al., 2016b, 2017; Pepe et al., 2019, 2020).

In the present work the focus is on anisotropic media and related simulations (Eremeyev and Pietraszkiewicz, 2016; Hasanyan and Waas, 2018). The interest on anisttropic media has been incresing in the recent years due to technology advancedments on industrial production and subsequent investigation (Eremeyev and Konopińska-Zmysłowska, 2020; Fahmy, 2021; Fahmy et al., 2021). Material characterization has been recently focused also on beams (structures where one dimension is larger than the other two) using nonlocal models (Apuzzo et al., 2019; Barretta et al., 2020; Taliercio and Veber, 2016). Nonlocal models demonstrated to be very effective in the analysis of nanostructures and nano composites (Acierno et al., 2017).

The present work considers previous knowledge of the authors on hexagonal assemblies with anisotropic nature as in Fantuzzi et al. (2019, 2020b) where novel material symmetries (Fantuzzi et al., 2020a) are analyzed. The aim of the work is to investigate the dynamic behavior of composite assemblies made of hexagonal particles as in Colatosti et al. (2021a) but by considering non-convex hexagonal shapes. This choice prove a fully anisotropic constitutive behavior of the equivalent material for a special selection of the geometric parameters. The validity of the homogenization procedure taken from the work by Trovalusci and Masiani (1999) is proven by considering a discrete finite element model and subsequently a parametric investigation is shown in order to demonstrated the peculiarity of

Cosserat modeling with respect to Cauchy when dynamics of these materials is under investigation.

The main structure of this work is listed below. After the introductory section, Cosserat theory is shortly detailed and main equations are reported together with the present finite element implementation considered in the following simulations. Numerical applications are detailed with reference to the present multiscale strategy and microscopic unit cell of the considered anisotropic class of materials. Discussions and conclusions are drawn at the end of the work.

2. COSSERAT CONTINUUM

As throughly discussed in the introductory section, many researchers showed that Cosserat theory can accurately model materials with microstructure (or materials with internal length) Forest et al. (1999); Leonetti et al. (2019); Trovalusci and Masiani (2003). In this work the analysis is restricted to the 2D framework, therefore the Cosserat model considers two displacements and one rotation (microrotation) as free parameters, whereas the classical Cauchy continuum has only two displacements. The linearized kinematic compatibility equations of the Cosserat model can be written as:

$$\varepsilon_{11} = u_{1,1}, \quad \varepsilon_{22} = u_{2,2}, \quad \varepsilon_{12} = u_{1,2} + \omega, \quad \varepsilon_{21} = u_{2,1} - \omega, \quad \chi_1 = \omega_{,1}, \quad \chi_2 = \omega_{,2} \tag{1}$$

where u_1 and u_2 are macro displacements components and ω is the microrotation. $\omega \neq \vartheta = 0.5(u_{2,1} - u_{1,2})$, thus relative rotation $\vartheta - \omega$ represents an interesting strain measure for checking the micropolar effect. ε_{ij} $(i,j = 1,2)$ are the strain components and χ_i $(i = 1,2)$ are curvatures in the Cosserat model and $\varepsilon_{12} \neq \varepsilon_{21}$. Subscripts $_{,1}$ and $_{,2}$ stand for the partial derivatives with respect to x_1 and x_2.

σ_{ij} and μ_i $(i,j = 1,2)$ are the work conjugated stress and microcouple measurements for ε_{ij} and χ_i, respectively, and $\sigma_{12} \neq \sigma_{21}$. Current notation for stress and strain measures are depicted in Fig. 1 (Tejchman and Górski (2006)). σ_{ij} and μ_i should satisfy the equilibrium at external boundary as $t_i = \sigma_{ij} n_j$ and $m_i = \mu_j n_j$, where t_i and m_i are the surface traction and moment traction, n_j collects the components of the outward normal to the boundary. Balance equations can be obtained from the virtual work principle (Trovalusci and Masiani (1999)):

$$\sigma_{ij,j} + b_i = 0, \quad \mu_{j,j} - e_{ij3}\sigma_{ij} = 0 \tag{2}$$

where b_i are the body force components, e_{ij3} is the permutation tensor (in the present case specified for the 2D framework).

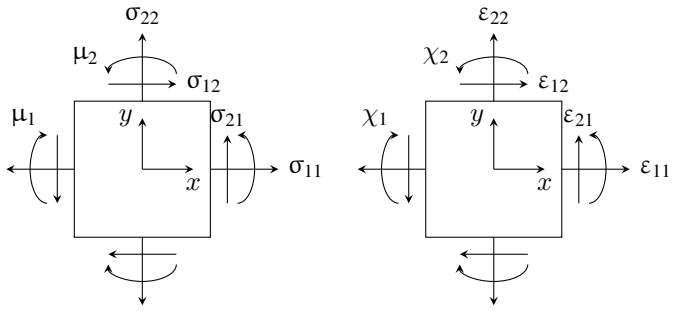

(a) σ_{ij} and μ_i (b) ε_{ij} and χ_i

FIG. 1: Plane differential elements of the Cosserat continuum.

Linear stress-strain relations for the Cosserat model can be written as:

$$\begin{Bmatrix} \sigma_{11} \\ \sigma_{22} \\ \sigma_{12} \\ \sigma_{21} \\ \mu_1 \\ \mu_2 \end{Bmatrix} = \begin{bmatrix} A_{1111} & A_{1122} & A_{1112} & A_{1121} & B_{111} & B_{112} \\ A_{2211} & A_{2222} & A_{2212} & A_{2221} & B_{221} & B_{222} \\ A_{1211} & A_{1222} & A_{1212} & A_{1221} & B_{121} & B_{122} \\ A_{2111} & A_{2122} & A_{2112} & A_{2121} & B_{211} & B_{212} \\ B_{111} & B_{122} & B_{112} & B_{121} & D_{11} & D_{12} \\ B_{211} & B_{222} & B_{212} & B_{221} & D_{21} & D_{22} \end{bmatrix} \begin{Bmatrix} \varepsilon_{11} \\ \varepsilon_{22} \\ \varepsilon_{12} \\ \varepsilon_{21} \\ \chi_1 \\ \chi_2 \end{Bmatrix} \tag{3}$$

where the constitutive matrix shows major symmetries if considering hyperelastic materials, i.e. $A_{ijhk} = A_{hkij}$, $B_{ijh} = B_{hij}$, $D_{ij} = D_{ji}$ $(i, j, h, k = 1, 2)$. The same matrices can be represented in matrix form by using the symbols $\mathbb{A}$, $\mathbb{B}$, and $\mathbb{D}$.

3. FINITE ELEMENT METHOD

A 2D displacement-based finite element method is considered. For Cosserat continua, the vector of model parameters is indicated as $\boldsymbol{d}$ which includes the displacement vector $\boldsymbol{u}$ and the microrotation vector $\boldsymbol{\omega}$ (that in the 2D case is a scalar, but it will be presented as in Leonetti et al. (2019)):

$$\boldsymbol{u}^\top = \begin{Bmatrix} u_1 & u_2 \end{Bmatrix}, \quad \boldsymbol{\omega} = \begin{Bmatrix} \omega \end{Bmatrix}, \quad \boldsymbol{d}^\top = \begin{Bmatrix} \boldsymbol{u}^\top & \boldsymbol{\omega} \end{Bmatrix} \tag{4}$$

Considering a domain $\mathcal{A}$ and boundary Γ, the weak form of the current problem (Leonetti et al. (2019); Shi et al.

(2021)) can be written as:

$$\int_{\mathcal{A}} \delta\boldsymbol{\varepsilon}^{\top}\boldsymbol{\sigma} + \delta\boldsymbol{\chi}^{\top}\boldsymbol{\mu}\, d\mathcal{A} = \int_{\mathcal{A}} \delta\boldsymbol{u}^{\top}\mathbf{b}\, d\mathcal{A} + \int_{\Gamma} \delta\boldsymbol{u}^{\top}\overline{\boldsymbol{t}} + \delta\boldsymbol{\omega}^{\top}\overline{\boldsymbol{m}}\, d\Gamma \qquad \forall\delta\boldsymbol{u}, \delta\boldsymbol{\omega} \tag{5}$$

where δ is the variational operator, $\boldsymbol{b}$ is the body force vector. $\overline{\boldsymbol{t}}$ and $\overline{\boldsymbol{m}}$ are the traction and couple-traction vectors applied on the boundary Γ. Different interpolating polynomials are used for the displacements and the microrotation. In particular, bi-quadratic ($\boldsymbol{N_u}$) and bi-linear ($\boldsymbol{N_\omega}$) shape functions are considered to approximate the classical displacements and microrotation respectively (Ferreira and Fantuzzi (2020); Leonetti et al. (2019)) as:

$$\boldsymbol{u} = \boldsymbol{N_u}\tilde{\boldsymbol{u}}, \quad \boldsymbol{\omega} = \boldsymbol{N_\omega}\tilde{\boldsymbol{\omega}} \tag{6}$$

where $\tilde{\boldsymbol{u}}$ and $\tilde{\boldsymbol{\omega}}$ are nodal displacement and microrotation values of each element.

$$\boldsymbol{\varepsilon} = \boldsymbol{L}\boldsymbol{u} + \boldsymbol{M}\boldsymbol{\omega}, \quad \boldsymbol{\chi} = \nabla\boldsymbol{\omega} \tag{7}$$

where, ∇ is the gradient operator, $\boldsymbol{L}$ and $\boldsymbol{M}$ can be expressed as:

$$\boldsymbol{L} = \begin{bmatrix} \frac{\partial}{\partial x_1} & 0 & \frac{\partial}{\partial x_2} & 0 \\ 0 & \frac{\partial}{\partial x_2} & 0 & \frac{\partial}{\partial x_1} \end{bmatrix}^{\top}, \quad \boldsymbol{M} = \begin{bmatrix} 0 & 0 & 1 & -1 \end{bmatrix}^{\top} \tag{8}$$

Substituting Eq. (6) into (7), the strain vectors become:

$$\boldsymbol{\varepsilon} = \boldsymbol{B_\varepsilon}\tilde{\boldsymbol{d}}, \quad \boldsymbol{\chi} = \boldsymbol{B_\chi}\tilde{\boldsymbol{d}} \tag{9}$$

where $\boldsymbol{B_\varepsilon}$ and $\boldsymbol{B_\chi}$ are the derivatives of the shape functions. $\tilde{\boldsymbol{d}}$ is the unknown vector of nodal displacements that follows the same order of $\boldsymbol{d}$ as indicated in eq. (4). Substituting Eq. (9) into Eq. (3), the constitutive relations become:

$$\boldsymbol{\sigma} = \mathbb{A}\boldsymbol{B_\varepsilon}\tilde{\boldsymbol{d}} + \mathbb{B}\boldsymbol{B_\chi}\tilde{\boldsymbol{d}}, \quad \boldsymbol{\mu} = \mathbb{B}^{\top}\boldsymbol{B_\varepsilon}\tilde{\boldsymbol{d}} + \mathbb{D}\boldsymbol{B_\chi}\tilde{\boldsymbol{d}} \tag{10}$$

By excluding body forces (only boundary loads will be considered in the following), the weak form Eq. (5) can be

expressed as:

$$\underbrace{\int_{\mathcal{A}^e} \left(\boldsymbol{B}_{\boldsymbol{\varepsilon}}^{\top}\mathbb{A}\boldsymbol{B}_{\boldsymbol{\varepsilon}} + \boldsymbol{B}_{\boldsymbol{\varepsilon}}^{\top}\mathbb{B}\boldsymbol{B}_{\boldsymbol{\chi}} + \boldsymbol{B}_{\boldsymbol{\chi}}^{\top}\mathbb{B}^{\top}\boldsymbol{B}_{\boldsymbol{\varepsilon}} + \boldsymbol{B}_{\boldsymbol{\chi}}^{\top}\mathbb{D}\boldsymbol{B}_{\boldsymbol{\chi}}\right) d\mathcal{A}^e}_{\boldsymbol{K}^e} \tilde{\boldsymbol{d}} = \underbrace{\int_{\Gamma^e} \begin{bmatrix} \boldsymbol{N}_{\boldsymbol{u}}^{\top}\overline{\boldsymbol{t}} & \boldsymbol{N}_{\boldsymbol{\omega}}^{\top}\overline{\boldsymbol{m}} \end{bmatrix}^{\top} d\Gamma^e}_{\boldsymbol{F}^e} \tag{11}$$

where $\boldsymbol{K}^e$ and $\boldsymbol{F}^e$ are the stiffness matrix and the nodal force vector of the element. The integral terms in Eq. (11) are computed numerically by a classical Gauss-Legendre integration with 3×3 grid.

4. NUMERICAL SIMULATIONS

In the following, a rectangular domain (fixed at the bottom edge and free on the other sides is considered) with width $L_x = 8.5$ μm and height $L_y = 12.9375$ μm is used to take numerical dynamic simulations. This rectangular domain is considered to be made of microstructured material with a density of $\rho = 10^{-6}$ μg/μm^3.

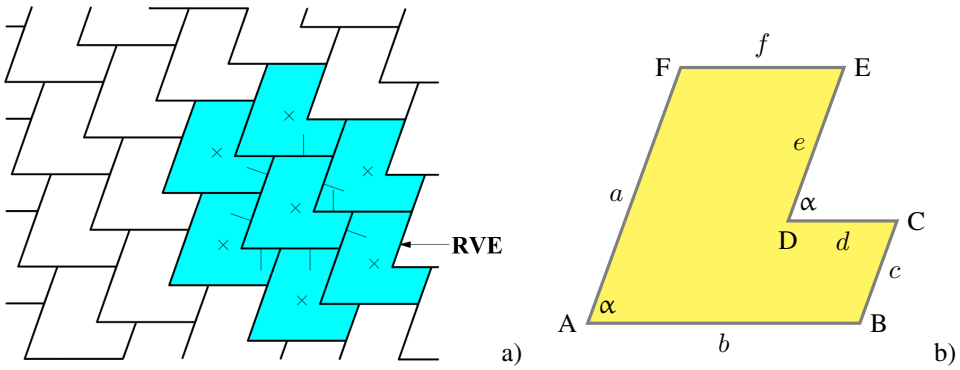

FIG. 2: a) General anisotropic assembly with RVE. b) Representative geometry of the anisotropic tile.

An assembly made of the irregular tiles organized according to the Representative Volume Element (RVE) given in Fig. 2a is considered in the following. A single tile, as shown in Fig. 2b, is defined by a parallelogram with a corner cutout. The geometry of the tile is determined by four parameters l_r, α, X, and Y, where l_r is the relative length defined as $\frac{l_r}{100} = \frac{b}{a+b}$, X and Y define the size of unfilled parallelogram corner, i.e. $\frac{X}{100} = \frac{d}{b}$ and $\frac{Y}{100} = \frac{e}{a}$. And $f = b - d, c = a - e$. The size/scale of the tile is identified by the parameter b, thus, Cartesian coordinates of the tile

by considering the origin in the point $A \equiv O$ they are given by:

$$
\begin{aligned}
A &= (0;\ 0) \\
B &= (b;\ 0) \\
C &= b\left(1 + \left(\frac{100}{l_r} - 1\right)\left(1 - \frac{Y}{100}\right)\cos\alpha;\ \left(\frac{100}{l_r} - 1\right)\left(1 - \frac{Y}{100}\right)\sin\alpha\right) \\
D &= b\left(1 - \frac{X}{100} + \left(\frac{100}{l_r} - 1\right)\left(1 - \frac{Y}{100}\right)\cos\alpha;\ \left(\frac{100}{l_r} - 1\right)\left(1 - \frac{Y}{100}\right)\sin\alpha\right) \\
E &= b\left(\left(\frac{100}{l_r} - 1\right)\cos\alpha + \left(1 - \frac{X}{100}\right);\ \left(\frac{100}{l_r} - 1\right)\sin\alpha\right) \\
F &= b\left(\left(\frac{100}{l_r} - 1\right)\cos\alpha;\ \left(\frac{100}{l_r} - 1\right)\sin\alpha\right)
\end{aligned}
\tag{12}
$$

It is clear from Eq. (12) that b represents the tile size/scale since it multiplies all geometric components. For the sake of clarity the following, b values for different scales s are defined as:

- $s = 1$ corresponds to $\frac{b}{L_x} \approx 0.0588$ (large tiles $b = \frac{1}{2}$);
- $s = \frac{3}{4}$ corresponds to $\frac{b}{L_x} \approx 0.04412$ (medium tiles $b = \frac{3}{8}$);
- $s = \frac{1}{4}$ corresponds to $\frac{b}{L_x} = 0.01471$ (small tiles $b = \frac{1}{8}$);

The tiles interact among elastic interfaces with normal component $K_{11} = 0.785$ mN/μm and shear component $K_{22} = 0.3925$ mN/μm. The homogenization approach by Trovalusci and Masiani (1999) can be applied by considering the RVE depicted in Figure 2.

4.1 Verification

In order to verify the present material modelling a simplified case is considered and then compared with a discrete model as in the previous works (Colatosti et al. (2021b)). The geometric parameters used in the present section are $l_r = X = Y = 50$ and $\alpha = 90°$. Thus, the Constitutive matrix (Eq. (3)) for the microstructure with $s = 1$ corresponds

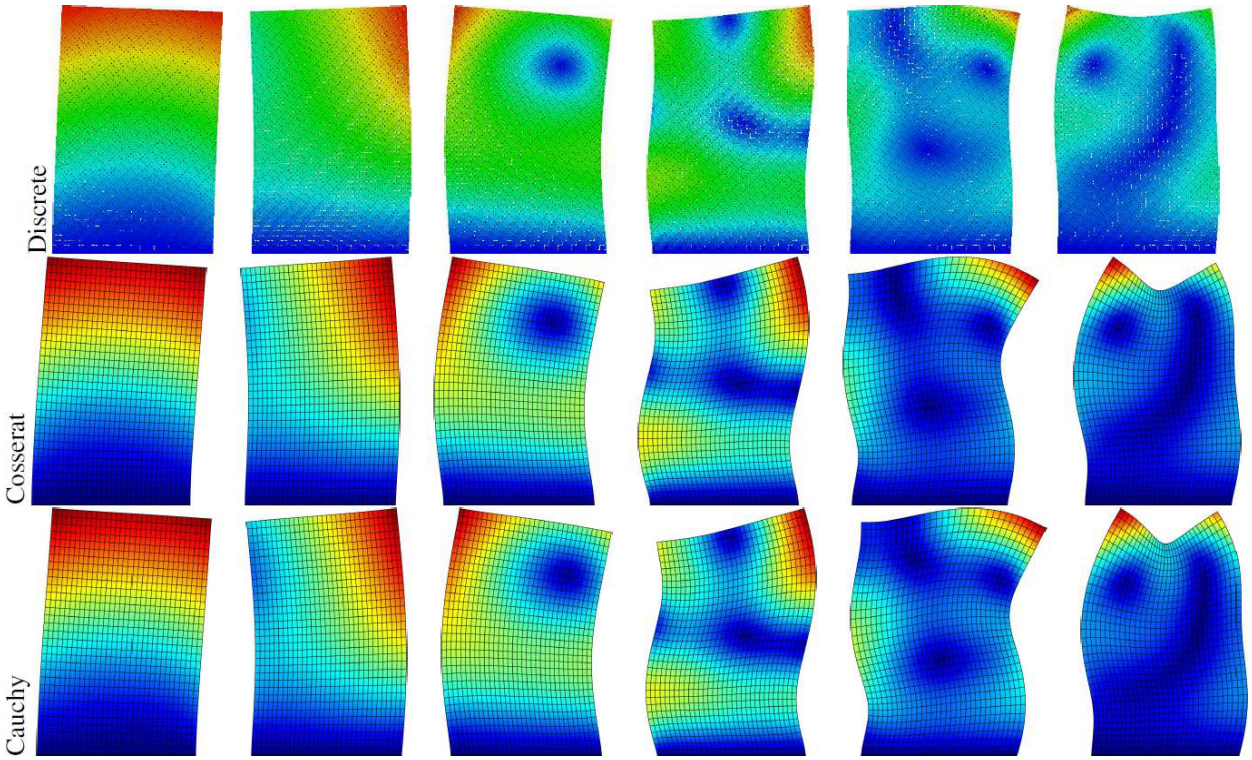

Vibration modes: microstructure scale $s = 1$.

to:

$$\mathbf{C}_{s=1} = \begin{bmatrix} 1.5700 & 0 & -0.3925 & 0 & -0.0491 & 0.0327 \\ 0 & 1.5700 & 0 & -0.3925 & -0.0327 & 0.0491 \\ -0.3925 & 0 & 1.1775 & 0 & 0.0327 & -0.0327 \\ 0 & -0.3925 & 0 & 1.1775 & 0.0327 & -0.0327 \\ -0.0491 & -0.0327 & 0.0327 & 0.0327 & 0.1043 & -0.0429 \\ 0.0327 & 0.0491 & -0.0327 & -0.0327 & -0.0429 & 0.0981 \end{bmatrix} \tag{13}$$

It can be noted from Eq. (13) that the present microstructure does not present Poisson effect (e.g. transverse contraction) but exhibits coupling between normal and shear components of stress/strains in $\mathbb{A}$ as well as full coupling because $\mathbb{B} \neq 0$ in all its components. The negligible Poisson effect is due to the chosen angle $\alpha = 90^\circ$ which reports horizontal and vertical geometric shape of each tile.

Results are depicted for the first 6 mode shapes in Figure 3 and frequency values are listed in Table 3 where relative error with respect to the discrete model are presented.

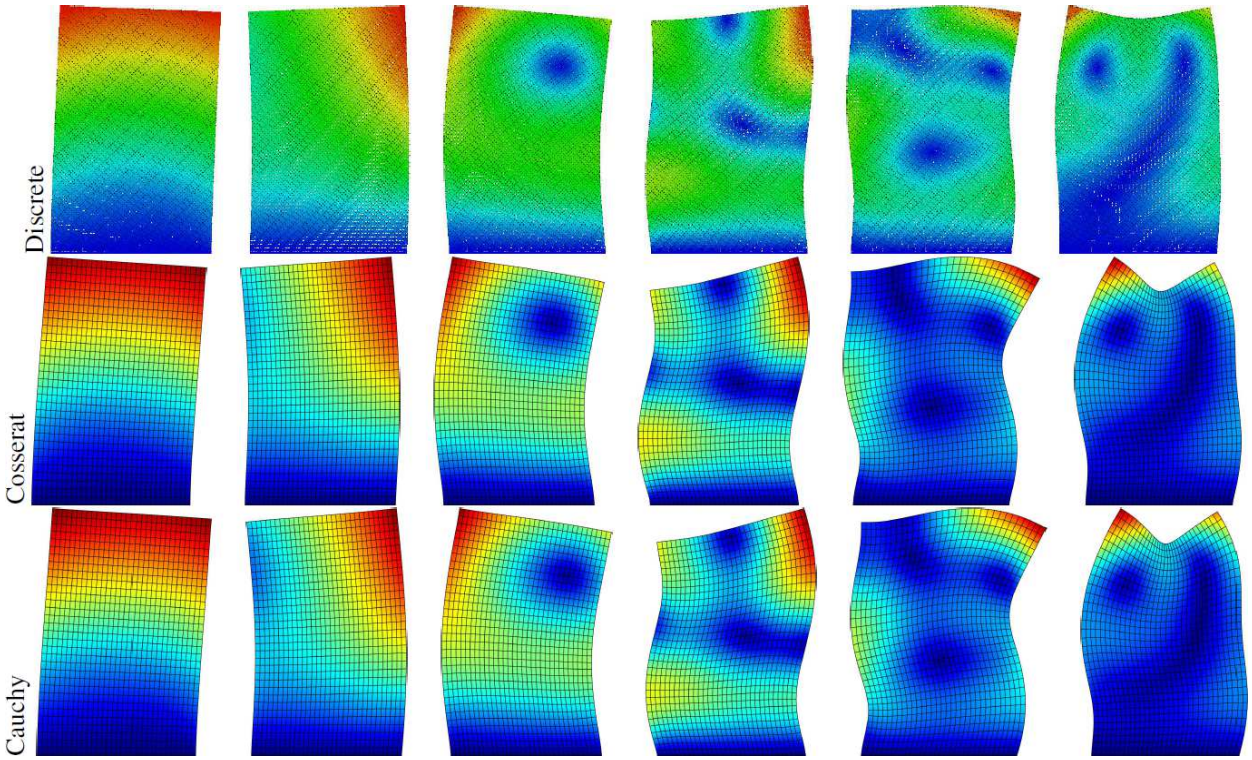

Vibration modes: microstructure scale $s = \frac{3}{4}$.

For the case considered, both Cosserat and Cauchy models represent accurately the dynamic behavior of the discrete model. Cauchy model is analyzed using the constitutive law as detailed in the appendix. This is due to the selected regular geometry which appear to have a major symmetry and the coupling effect due to matrix $\mathbb{B} \neq 0$ not relevant as well as scale matrix $\mathbb{D} \neq 0$. Therefore, it is expected to have similar behavior for the other smaller scales which generally tends to behave like a Cauchy continuum (Colatosti et al. (2021b)).

TABLE 1: Natural frequencies scale $s = 1$

Mode	Discrete (MHz)	Cosserat (MHz)	Error (%)	Cauchy (MHz)	Error (%)
1	8.0158	7.8223	2.4140	7.8542	2.0160
2	23.371	22.9166	1.9443	23.1925	0.7638
3	27.158	26.5713	2.1603	26.7215	1.6073
4	50.941	50.6451	0.9935	50.2650	1.3270
5	59.241	58.6451	1.0059	58.8080	-0.7309
6	64.253	63.2484	1.5635	64.7447	-0.7653

The Constitutive matrix (Eq. (3)) for the microstructure with $s = \frac{3}{4}$ corresponds to:

$$\mathbf{C}_{s=3/4} = \begin{bmatrix} 1.5700 & 0 & -0.3925 & 0 & -0.0368 & 0.0327 \\ 0 & 1.5700 & 0 & -0.3925 & -0.0245 & 0.0368 \\ -0.3925 & 0 & 1.1775 & 0 & 0.0245 & -0.0245 \\ 0 & -0.3925 & 0 & 1.1775 & 0.0245 & -0.0245 \\ -0.0368 & -0.0245 & 0.0245 & 0.0245 & 0.0586 & -0.0241 \\ 0.0245 & 0.0368 & -0.0245 & -0.0245 & -0.0241 & 0.0552 \end{bmatrix} \tag{14}$$

As mentioned in the previous works by Trovalusci and Masiani (1999); Trovalusci and Pau (2014). A change in the scale results in a change of matrices $\mathbb{B}$ and $\mathbb{D}$, whereas matrix $\mathbb{A}$ is unchanged.

Comparison in terms of natural frequencies in depicted in Figure 4 for the first 6 mode shapes. The same in terms of frequency is listed with the correspondent relative error in Table 2.

As aforementioned, the results show good agreement between Cosserat and Cauchy models with respect to the reference discrete one.

Finally, the constitutive matrix for the microstructure $s = \frac{1}{4}$ is given:

$$\mathbf{C}_{s=1/4} = \begin{bmatrix} 1.5700 & 0 & -0.3925 & 0 & -0.0123 & 0.0082 \\ 0 & 1.5700 & 0 & -0.3925 & -0.0082 & 0.0123 \\ -0.3925 & 0 & 1.1775 & 0 & 0.0082 & -0.0082 \\ 0 & -0.3925 & 0 & 1.1775 & 0.0082 & -0.0082 \\ -0.0123 & -0.0082 & 0.0082 & 0.0082 & 0.0065 & -0.0027 \\ 0.0082 & 0.0123 & -0.0082 & -0.0082 & -0.0027 & 0.0061 \end{bmatrix} \tag{15}$$

The results in terms of mode shapes are depicted in Figure 5 and compared among discrete, Cosserat and Cauchy

TABLE 2: Natural frequencies scale $s = \frac{3}{4}$

Mode	Discrete (MHz)	Cosserat (MHz)	Error (%)	Cauchy (MHz)	Error (%)
1	8.0709	7.7939	3.4321	7.8542	2.6850
2	23.39	22.8794	2.1997	23.1925	0.8613
3	27.243	26.5317	2.6109	26.7215	1.9143
4	51.023	50.3142	1.3892	50.2650	1.4856
5	60.415	58.6227	2.9666	58.8080	2.6599
6	66.454	63.4760	4.4813	64.7447	2.5722

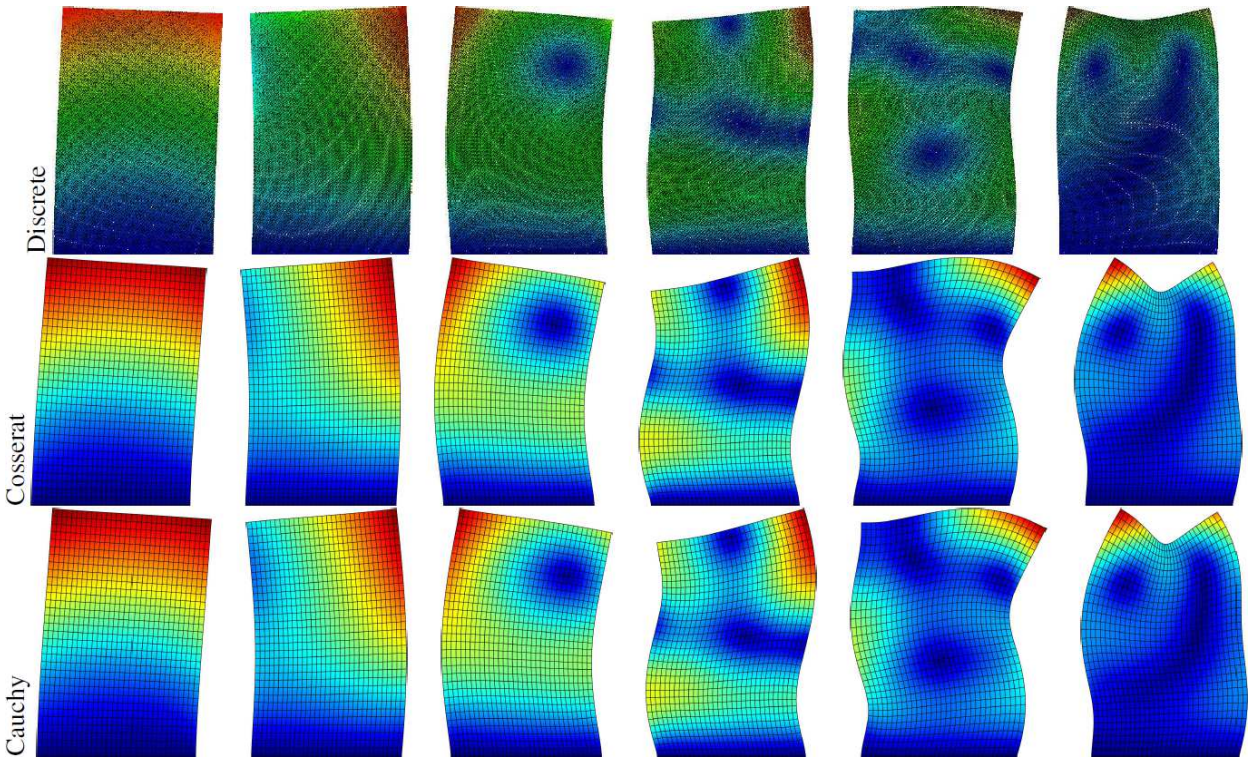

Vibration modes: microstructure scale $s = \frac{1}{4}$.

models. The same in terms of vibration frequency is listed in Table 3. Once again the results all agree well with respect to the discrete model.

4.2 Parametric investigation

In this section, a parametric investigation in order to analyze the effects of three parameters α, X and Y are reported according to the following three selections:

1. Effect of α: $l_r = 50, X = 50, Y = 50, \alpha = 30^\circ \sim 150^\circ$ with an interval of 10°.

TABLE 3: Natural frequencies scale $s = \frac{1}{4}$

Mode	Discrete (MHz)	Cosserat (MHz)	Error (%)	Cauchy (MHz)	Error (%)
1	7.7780	7.7500	0.3600	7.8542	-0.9797
2	22.646	22.7984	-0.6730	23.1925	-2.4132
3	26.208	26.4477	-0.9146	26.7215	-1.9593
4	48.934	50.0730	-2.3276	50.2650	-2.7200
5	57.428	58.4539	-1.7864	58.8080	-2.4030
6	62.581	63.6443	-1.6991	64.7447	-3.4574

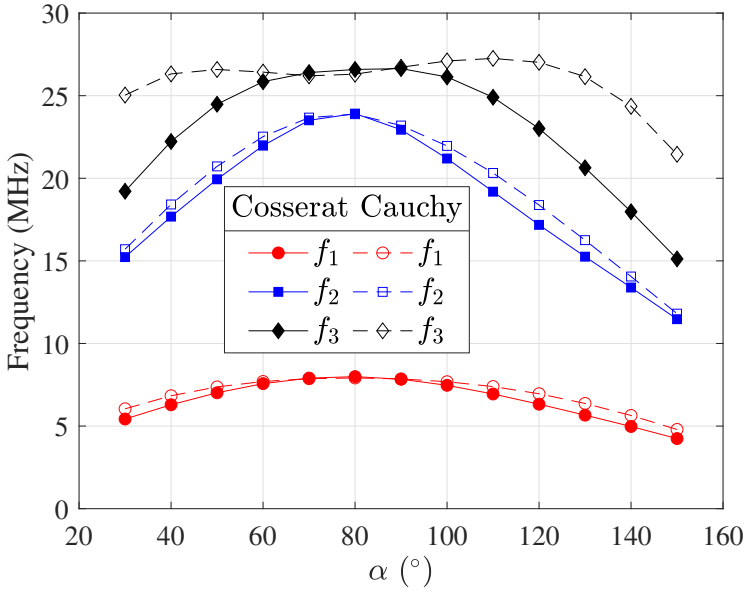

FIG. 6: First 3 frequencies as a function of parameter α.

2. Effect of X: $l_r = 50, \alpha = 90°, Y = 50, X = 20 \sim 80$ with an interval of 10.

3. Effect of Y: $l_r = 50, \alpha = 90°, X = 50, Y = 20 \sim 80$ with an interval of 10.

Free vibration tests are performed on the rectangular domain mentioned above using both Cosserat and Cauchy continua. The first 3 frequencies are used to evaluate the effects of the parameters.

Fig. 6 shows the first 3 frequencies as a function of the angle α. Frequencies f_1 and f_2 have little difference between Cosserat and Cauchy continuum. These two frequencies firstly increase and then decrease with the α for both models. The highest f_1 and f_2 can be found when $\alpha = 80°$. Similar behavior can be also observed for f_3 from the Cosserat continuum, whereas f_3 from the Cauchy continuum has no obvious trend with α, resulting in big difference in this frequencies between the two models. All 3 frequencies from the two continuum coincide well when α is close to 80° (also also shown in the verification section more in detail) but show more or fewer differences as α departs from 80°.

Fig. 7 shows the effect of parameter X on the first 3 frequencies. All 3 frequencies from the two continuum coincide well when $X \leq 50$ (as shown also in the verification section), whereas when $X > 50$ the difference between two continuum become larger as X increases. Such differences are greater in f_2 and f_3 than that in f_1. Similar behavior can be also found when $Y \leq 50$ and $Y > 50$ (Fig. 8). However, these three frequencies behave differently as X and Y increase. Actually, f_1 changes slightly with both X and Y. f_2 from Cosserat and Cauchy continuum both increase slightly and then decrease with X, whereas they decrease monotonously with increasing Y.

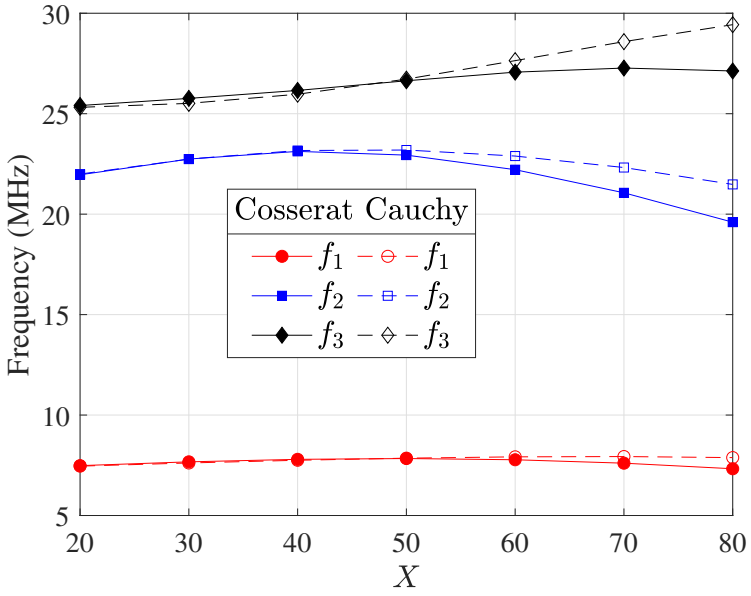

FIG. 7: First 3 frequencies as a function of parameter X.

f_3 shows the highest difference between two continuum if X and Y have high values. As X increases, f_3 of Cosserat continuum increases firstly and then decreases, whereas that of Cauchy continuum keep increasing. As Y increases, f_3 of Cosserat continuum changes slightly, whereas that of Cauchy continuum has a obvious increase trend when $Y > 50$.

For better investigate the change in frequency as parameter varies, Tables 4-6 calculate the relative error of above frequencies with respect to a reference parameter configuration. The reference configurations has $90°, 50$ and 50 for parameters α, X and Y, respectively. It can be seen that α has a greater effect on the relative change in the frequency than X and Y. By varying α results in the highest relative error that near to -50%. Such a value is only -14.55% and -11.03% when changing X and Y, respectively. In general, for all the three parameters, as the configuration departs from its corresponding reference configuration, the relative error of frequency increases. Table. 4 indicates that the change in frequency as α is more relevant in the Cosserat continuum than in the Cauchy one for all three frequencies.

TABLE 4: Effect of parameter α on first 3 frequencies: relative error with respect to $\alpha = 90°$ (%).

		α						
Freq.	models	30°	50°	70°	90°	110°	130°	150°
f_1	Cosserat	-30.74	-10.47	0.87	0	-11.40	-27.74	-45.84
	Cauchy	-23.04	-6.16	0.17	0	-5.89	-18.89	-38.95
f_2	Cosserat	-33.61	-13.08	2.50	0	-16.35	-33.49	-49.99
	Cauchy	-32.28	-10.66	2.07	0	-12.37	-29.91	-49.10
f_3	Cosserat	-27.87	-8.10	-0.90	0	-6.52	-22.53	-43.25
	Cauchy	-6.31	-0.51	-1.95	0	2.00	-2.13	-19.73

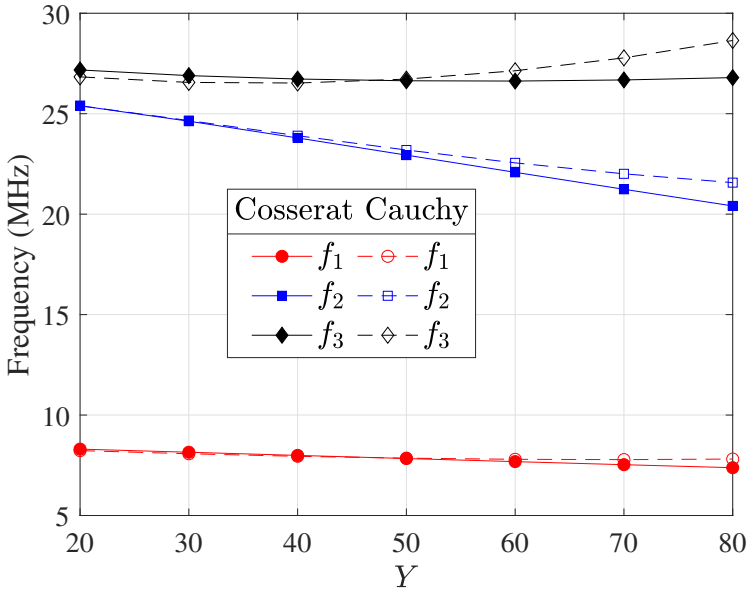

FIG. 8: First 3 frequencies as a function of parameter Y.

f_2 changes the most, followed by f_1 and then f_3.

As for varying X (Table. 5), the highest relative error (-14.35%) is also observed for f_2 when $X = 80$ using Cosserat continuum. Only for f_3, it is shown that the relative error is greater in the Cauchy continuum than in the Cosserat one for all configurations. Effect of continuum used on the relative error in f_1 and f_2 seems uncertain for different configurations. On the contrary, Table 6 shows that for f_1 and f_2 the relative change in frequency is significant in the Cosserat continuum than in the Cauchy one. And the effect of continuum is uncertain for f_3 as Y changes. In general, by varying Y can result in the most significant relative change in f_2, followed by f_1 and then f_3. Exception is made in the Cauchy continuum when $Y > 50$, where the relative change in f_2 is the greatest but followed by f_3 and then f_1.

In conclusion, as the investigated parameters vary, there is small difference in low frequency (f_1) between the Cosserat and Cauchy continuum, whereas such a difference become larger for high frequencies (f_2 and f_3) especially

TABLE 5: Effect of parameter X on first 3 frequencies: relative error with respect to $X = 50$ (%).

		X						
Freq.	models	20	30	40	50	60	70	80
f_1	Cosserat	-4.51	-2.10	-0.51	0	-0.78	-2.95	-6.49
	Cauchy	-5.05	-3.04	-1.33	0	0.84	1.02	0.35
f_2	Cosserat	-4.27	-0.86	0.81	0	-3.16	-8.18	-14.55
	Cauchy	-5.17	-1.94	-0.11	0	-1.30	-3.76	-7.38
f_3	Cosserat	-4.62	-3.29	-1.80	0	1.61	2.38	1.84
	Cauchy	-5.25	-4.52	-2.82	0	3.44	6.98	10.14

when α departs from 80°, $X > 50$, and $Y > 50$. The parameter α has the highest effect on the relative change in frequencies comparing with effects of X and Y, which means that α also largely influence the tile's degree of anisotropy. All three investigated parameters result in the highest effect on the relative change in f_2. Although f_1 is the smallest in value, the relative changes in f_1 as parameters are comparable with other frequencies. Since the low frequency plays an important role in dynamic analysis, such an effect of parameter on the change in f_1 should be noted.

5. CONCLUSIONS

This work presented a multiscale homogenization of anisotropic nanocomposites made of non-convex hexagonal assemblies. Homogenized material properties are included in a continuum Cosserat model and compared with a classical Cauchy model and a reference discrete configuration in free vibration. A parametric investigation is conducted in order to provide details on how the material symmetries are influenced by the non-convex geometries considered. Interlocking and tile distortion result to play a fundamental role in Cosserat media as previously discussed in previous work, however, in this paper for the first time such aspects are demonstrated via numerical applications.

ACKNOWLEDGMENTS

The second author acknowledges the support from China Scholarship Council (CSC) for providing funds (No. 202006050138).

TABLE 6: Effect of parameter Y on first 3 frequencies: relative error with respect to $Y = 50$ (%).

		Y						
Freq.	models	20	30	40	50	60	70	80
f_1	Cosserat	5.98	4.00	1.99	0	-1.97	-3.91	-5.82
	Cauchy	4.79	2.80	1.19	0	-0.72	-0.92	-0.57
f_2	Cosserat	10.71	7.36	3.73	0	-3.73	-7.41	-11.03
	Cauchy	9.50	6.32	3.07	0	-2.76	-5.11	-7.00
f_3	Cosserat	2.02	0.96	0.33	0	-0.05	0.16	0.59
	Cauchy	0.42	-0.62	-0.73	0	1.55	3.96	7.19

APPENDIX A. CAUCHY CONSTITUTIVE MATRIX

In this section the Cauchy constitutive matrix is derived from the Cosserat homogenized constitutive relation (Eq. (3)) according to the notation provided in the work by Trovalusci et al. (2015). Starting from the strain definitions in 2D:

$$\varepsilon_{ij} = u_{i,j} + e_{3ij}\omega, \quad \chi_3 j = \omega_{,j} \tag{A.1}$$

where $i, j = 1, 2$ and e_{3ij} is the Levi-Civita symbol. If the classical and micropolar components are identified as symmetric and antisymmetric parts of the strain and stress tensors as:

$$\varepsilon_{ij} = \varepsilon^S_{ij} + \varepsilon^A_{ij}, \quad \sigma_{ij} = \sigma^S_{ij} + \sigma^A_{ij} \tag{A.2}$$

where subscripts ^{S} and ^{A} indicate symmetric and skew-symmetric parts of the tensors and

$$\begin{aligned} \varepsilon^S_{ij} &= \frac{1}{2}\left(u_{i,j} + u_{j,i}\right), \quad \varepsilon^A_{ij} = \frac{1}{2}\left(u_{i,j} - u_{j,i}\right) + e_{3ij}\omega \\ \sigma^S_{ij} &= \frac{1}{2}\left(\sigma_{ij} + \sigma_{ji}\right), \quad \sigma^A_{ij} = \frac{1}{2}\left(\sigma_{ij} - \sigma_{ji}\right) \end{aligned} \tag{A.3}$$

from equation (A.3) with $i = 1$ and $j = 2$ the following can be carried out

$$u_{1,2} = 2\varepsilon^S_{12} - u_{2,1}, \quad \omega = -\frac{1}{2}\left(u1,2 - u_{2,1}\right) + \varepsilon^A_{12} \tag{A.4}$$

by substituting definitions (A.4) in Eq. (3) it results:

$$\begin{aligned} \sigma_{11} &= A_{1111}\varepsilon_{11} + A_{1122}\varepsilon_{22} - A_{1121}(\varepsilon^A_{12} - \varepsilon^S_{12}) + A_{1112}(\varepsilon^A_{12} + \varepsilon^S_{12}) \\ \sigma_{22} &= A_{1122}\varepsilon_{11} + A_{2222}\varepsilon_{22} - A_{2221}(\varepsilon^A_{12} - \varepsilon^S_{12}) + A_{2212}(\varepsilon^A_{12} + \varepsilon^S_{12}) \\ \sigma_{12} &= A_{1112}\varepsilon_{11} + A_{2212}\varepsilon_{22} - A_{1221}(\varepsilon^A_{12} - \varepsilon^S_{12}) + A_{1212}(\varepsilon^A_{12} + \varepsilon^S_{12}) \\ \sigma_{21} &= A_{1121}\varepsilon_{11} + A_{2221}\varepsilon_{22} - A_{2121}(\varepsilon^A_{12} - \varepsilon^S_{12}) + A_{1221}(\varepsilon^A_{12} + \varepsilon^S_{12}) \end{aligned} \tag{A.5}$$

it is noted that $\varepsilon_{ii} = \varepsilon_{ii}^S = u_{i,i}$. Such relationships can be rewritten as:

$$\begin{aligned}
\sigma_{11} &= A_{1111}\varepsilon_{11} + A_{1122}\varepsilon_{22} + (A_{1112} + A_{1121})\varepsilon_{12}^S + (A_{1112} - A_{1121})\varepsilon_{12}^A \\
\sigma_{22} &= A_{1122}\varepsilon_{11} + A_{2222}\varepsilon_{22} + (A_{2221} + A_{2212})\varepsilon_{12}^S + (A_{2212} - A_{2221})\varepsilon_{12}^A \\
\sigma_{12}^S &= \frac{A_{1112} + A_{1121}}{2}\varepsilon_{11} + \frac{A_{2212} + A_{2221}}{2}\varepsilon_{22} + \frac{A_{1212} + 2A_{1221} + A_{2121}}{2}\varepsilon_{12}^S + \frac{A_{1212} - A_{2121}}{2}\varepsilon_{12}^A \\
\sigma_{12}^A &= \frac{A_{1112} - A_{1121}}{2}\varepsilon_{11} + \frac{A_{2212} - A_{2221}}{2}\varepsilon_{22} + \frac{A_{1212} - A_{2121}}{2}\varepsilon_{12}^S + \frac{A_{1212} - 2A_{1221} + A_{2121}}{2}\varepsilon_{12}^A
\end{aligned} \tag{A.6}$$

Since in the Cauchy continuum $2\varepsilon_{12}^S = \gamma_{12}$ and $\varepsilon_{12}^A = 0$ constitutive matrix for the Cauchy continuum can be derived:

$$\begin{Bmatrix} \sigma_{11} \\ \sigma_{22} \\ \sigma_{12}^S \end{Bmatrix} = \begin{bmatrix} A_{1111} & A_{1122} & \frac{1}{2}(A_{1112} + A_{1121}) \\ A_{1122} & A_{2222} & \frac{1}{2}(A_{2221} + A_{2212}) \\ \frac{1}{2}(A_{1112} + A_{1121}) & \frac{1}{2}(A_{2212} + A_{2221}) & \frac{1}{4}(A_{1212} + 2A_{1221} + A_{2121}) \end{bmatrix} \begin{Bmatrix} \varepsilon_{11} \\ \varepsilon_{22} \\ \gamma_{12} \end{Bmatrix} \tag{A.7}$$

It is noted that the constitutive matrix is symmetric as it is expected from the theory. Constitutive matrix (A.7) is the one used in the computations as Cauchy continuum.

REFERENCES

Acierno, S., Barretta, R., Luciano, R., Marotti de Sciarra, F., and Russo, P., Experimental Evaluations and Modeling of the Tensile Behavior of Polypropylene/Single-Walled Carbon Nanotubes Fibers, *Compos. Struct.*, vol. **174**, pp. 12–18, 2017.

Adhikary, D. and Dyskin, A., A Cosserat Continuum Model for Layered Materials, *Comput. Geotech.*, vol. **20**, no. 1, pp. 15–45, 1997.

Adhikary, D.P., Mühlhaus, H.B., and Dyskin, A.V., Modelling the Large Deformations in Stratified Media—The Cosserat Continuum Approach, *Mech. Cohesive-Frictional Mater.*, vol. **4**, no. 3, pp. 195–213, 1999.

Apuzzo, A., Barretta, R., Fabbrocino, F., Faghidian, S.A., Luciano, R., and Marotti de Sciarra, F., Axial and Torsional Free Vibrations of Elastic Nano-Beams by Stress-Driven Two-Phase Elasticity, *J. Appl. Comput. Mech*., vol. **5**, no. 2, pp. 402–413, 2019.

Barretta, R., Fabbrocino, F., Luciano, R., de Sciarra, F.M., and Ruta, G., Buckling Loads of Nano-Beams in Stress-Driven Nonlocal Elasticity, *Mech. Adv. Mater. Struct*., vol. **27**, no. 11, pp. 869–875, 2020.

Bassani, J., Needleman, A., and Van der Giessen, E., Plastic Flow in a Composite: A Comparison of Nonlocal Continuum and Discrete Dislocation Predictions, *Int. J. Solids Struct*., vol. **38**, no. 5, pp. 833–853, 2001.

Bažant, Z., Belytschko, T., and Chang, T., Continuum Theory for Strain-Softening, *J. Eng. Mech. ASCE*, vol. **110**, no. 12, pp. 1666–1692, 1984.

Blanc, X., Le Bris, C., and Lions, P.L., From Molecular Models to Continuum Mechanics, *Arch. Rational Mech. Anal*., vol. **164**, no. 4, pp. 341–381, 2002.

Budiansky, B., On the Elastic Moduli of Some Heterogeneous Materials, *J. Mech. Phys. Solids*,

vol. **13**, no. 4, pp. 223–227, 1965.

Cermelli, P. and Pastrone, F., Shear Waves in Micro-Faulted Materials, Wave Motion, vol. **34**, no. 1, pp. 27–33, 2001.

Cimmelli, V., Oliveri, F., and Pace, A., Thermodynamical Setting for Gradient Continuum Theories with Vectorial Internal Variables: Application to Granular Materials, *Int. J. Non-Linear Mech.*, vol. **49**, pp. 72–76, 2013.

Colatosti, M., Fantuzzi, N., and Trovalusci, P., Dynamic Characterization of Microstructured Materials Made of Hexagonal-Shape Particles with Elastic Interfaces, *Nanomaterials*, vol. **11**, no. 7, 2021a.

Colatosti, M., Fantuzzi, N., Trovalusci, P., and Masiani, R., New Insights on Homogenization for Hexagonal-Shaped Composites as Cosserat Continua, *Meccanica*, 2021b.

Cowin, S., Stress Functions for Cosserat Elasticity, *Int. J. Solids Struct*., vol. **6**, no. 4, pp. 389–398, 1970.

Curtin, W.A. and Miller, R.E., Atomistic/Continuum Coupling in Computational Materials Science, *Model. Simul. Mater. Sci. Eng.*, vol. **11**, no. 3, pp. R33–R68, 2003.

De Borst, R., Simulation of Strain Localization: A Reappraisal of the Cosserat Continuum, vol. **8**, no. 4, pp. 317–332, 1991.

De Borst, R. and Mühlhaus, H.B., Gradient-Dependent Plasticity: Formulation and Algorithmic Aspects, *Int. J. Numer. Methods Eng*., vol. **35**, no. 3, pp. 521–539, 1992.

Eremeyev, V.A. and Konopińska-Zmysłowska, V., On Dynamic Extension of a Local Material Symmetry Group for Micropolar Media, *Symmetry*, vol. **12**, no. 10, 2020.

Eremeyev, V.A. and Pietraszkiewicz, W., Material Symmetry Group and Constitutive Equations of Micropolar Anisotropic Elastic Solids, *Math. Mech. Solids*, vol. **21**, no. 2, pp. 210–221, 2016.

Ericksen, J.L. and Truesdell, C., Exact Theory of Stress and Strain in Rods and Shells, *Arch. Rational Mech. Anal*., vol. **1**, no. 1, pp. 295–323, 1957.

Eringen, A., Linear Theory of Nonlocal Elasticity and Dispersion of Plane Waves, *Int. J. Eng. Sci.*, vol. **10**, no. 5, pp. 425–435, 1972.

Eringen, A.C., On Differential Equations of Nonlocal Elasticity and Solutions of Screw Dislocation and Surface Waves, *J. Appl. Phys*., vol. **54**, no. 9, pp. 4703–4710, 1983.

Fahmy, M.A., A Novel Bem for Modeling and Simulation of 3t Nonlinear Generalized Anisotropic Micropolar-Thermoelasticity Theory with Memory Dependent Derivative, *Comput. Model. Eng. Sci*., vol. **126**, no. 1, pp. 175–199, 2021.

Fahmy, M.A., Shaw, S., Mondal, S., Abouelregal, A.E., Lotfy, K., Kudinov, I.A., and Soliman, A.H., Boundary Element Modeling for Simulation and Optimization of Three-Temperature Anisotropic Micropolar Magneto-Thermoviscoelastic Problems in Porous Smart Structures Using Nurbs and Genetic Algorithm, *Int. J. Thermophys*., vol. **42**, no. 2, p. 29, 2021.

Fantuzzi, N., Trovalusci, P., and Dharasura, S., Mechanical Behavior of Anisotropic Composite Materials as Micropolar Continua, *Front. Mater*., vol. **6**, p. 59, 2019.

Fantuzzi, N., Trovalusci, P., and Luciano, R., Material Symmetries in Homogenized Hexagonal-Shaped Composites as Cosserat Continua, *Symmetry*, vol. **12**, no. 3, 2020a.

Fantuzzi, N., Trovalusci, P., and Luciano, R., Multiscale Analysis of Anisotropic Materials with Hexagonal Microstructure as Micropolar Continua, *Int. J. Multiscale Comput. Eng.*, vol. **18**, no. 2, pp. 265–284, 2020b.

Ferreira, A.J. and Fantuzzi, N., *MATLAB Codes for Finite Element Analysis: Solids and Structures*, Second Ed., Berlin: Springer, 2020.

Forest, S., Dendievel, R., and Canova, G.R., Estimating the Overall Properties of Heterogeneous

Cosserat Materials, *Model. Simul. Mater. Sci. Eng*., vol. **7**, no. 5, pp. 829–840, 1999.

Gerolymatou, E., A Micromechanically Derived Anisotropic Micropolar Constitutive Law for Granular Media: Elasticity, *Int. J. Numer. Anal. Methods Geomech*., vol. **38**, no. 17, pp. 1761–1775, 2014.

Greco, F., Leonetti, L., Luciano, R., and Blasi, P.N., Effects of Microfracture and Contact Induced Instabilities on the Macroscopic Response of Finitely Deformed Elastic Composites, *Compos. Part B: Eng*., vol. **107**, pp. 233–253, 2016a.

Greco, F., Leonetti, L., Luciano, R., and Nevone Blasi, P., An Adaptive Multiscale Strategy for the Damage Analysis of Masonry Modeled as a Composite Material, *Compos. Struct*., vol. **153**, pp. 972–988, 2016b.

Greco, F., Leonetti, L., Luciano, R., and Trovalusci, P., Multiscale Failure Analysis of Periodic Masonry Structures with Traditional and Fiber-Reinforced Mortar Joints, *Compos. Part B: Eng*., vol. **118**, pp. 75–95, 2017.

Green, A.E. and Rivlin, R.S., *On Cauchy's Equations of Motion*, New York: Springer New York, pp. 1359–1361, 1997.

Gurtin, M.E. and Podio-Guidugli, P., On the Formulation of Mechanical Balance Laws for Structured Continua, *Zeitschrift für angewandte Mathematik und Physik ZAMP*, vol. **43**, no. 1, pp. 181–190, 1992.

Hasanyan, A. and Waas, A., Localization in Anisotropic Elastoplastic Micropolar Media: Application to fiber Reinforced Composites, *J. Mech. Phys. Solids*, vol. **121**, pp. 1–22, 2018.

Jain, J.R. and Ghosh, S., Damage Evolution in Composites with a Homogenization-Based Continuum Damage Mechanics Model, *Int. J. Damage Mech*., vol. **18**, no. 6, pp. 533–568, 2009.

Kröner, E., On the Physical Reality of Torque Stresses in Continuum Mechanics, *Int. J. Eng.*

Sci., vol. **1**, no. 2, pp. 261–278, 1963.

Kumar, R., Sharma, N., and Ram, P., Interfacial Imperfection on Reflection and Transmission of Plane Waves in Anisotropic Micropolar Media, *Theor. Appl. Fract. Mech*., vol. **49**, no. 3, pp. 305–312, 2008.

Kunin, I., Elastic *Media with Microstructure II: Three-Dimensional Models*, Springer Series in Solid-State Sciences, Berlin: Springer, 2012.

Leonetti, L., Fantuzzi, N., Trovalusci, P., and Tornabene, F., Scale Effects in Orthotropic Composite Assemblies as Micropolar Continua: A Comparison between Weak- and Strong-Form Finite Element Solutions, *Materials*, vol. **12**, no. 5, 2019.

Li, J. and Ostoja-Starzewski, M., Micropolar Continuum Mechanics of Fractal Media, *Int. J. Eng. Sci.*, vol. **49**, no. 12, pp. 1302–1310, 2011.

Li, Y.P., Yang, C.H., Daemen, J.J.K., Yin, X.Y., and Chen, F., A New Cosserat-Like Constitutive Model for Bedded Salt Rocks, *Int. J. Numer. Anal. Methods Geomech*., vol. **33**, no. 15, pp. 1691–1720, 2009.

Lu, W., Zhu, Z., Que, X., Zhang, C., and He, Y., Anisotropic Constitutive Model of Intermittent Columnar Jointed Rock Masses Based on the Cosserat Theory, *Symmetry*, vol. **12**, no. 5, 2020.

Luciano, R. and Barbero, E.J., Analytical Expressions for the Relaxation Moduli of Linear Viscoelastic Composites With Periodic Microstructure, *J. Appl. Mech*., vol. **62**, no. 3, pp. 786–793, 1995.

Luciano, R. and Willis, J., Bounds on Non-Local Effective Relations for Random Composites Loaded by Configuration-Dependent Body Force, *J. Mech. Phys. Solids*, vol. **48**, no. 9, pp. 1827–1849, 2000.

Luciano, R. and Willis, J., Boundary-Layer Corrections for Stress and Strain Fields in Randomly

Heterogeneous Materials, *J. Mech. Phys. Solids*, vol. **51**, no. 6, pp. 1075–1088, 2003.

Luciano, R. and Willis, J., Fe Analysis of Stress and Strain Fields in Finite Random Composite Bodies, *J. Mech. Phys. Solids*, vol. **53**, no. 7, pp. 1505–1522, 2005.

Luciano, R. and Willis, J.R., Hashin–Shtrikman Based Fe Analysis of the Elastic Behaviour of Finite Random Composite Bodies, *Int. J. Fract*., vol. **137**, no. 1, pp. 261–273, 2006.

Luding, S., Anisotropy in Cohesive, Frictional Granular Media, *J. Phys.: Condensed Matter*, vol. **17**, no. 24, pp. S2623–S2640, 2005.

Makowski, J. and Stumpf, H., Thermodynamically Based Concept for the Modelling of Continua with Microstructure and Evolving Defects, *Int. J. Solids Struct.*, vol. **38**, no. 10, pp. 1943–1961, 2001.

Mariano, P.M. and Trovalusci, P., Constitutive Relations for Elastic Microcracked Bodies: From a Lattice Model to a Multifield Continuum Description, *Int. J. Damage Mech*., vol. **8**, no. 2, pp. 153–173, 1999.

Maugin, G., *Non-Classical Continuum Mechanics: A Dictionary, Advanced Structured Materials*, Singapore: Springer, 2016.

Mindlin, R.D., Micro-Structure in Linear Elasticity, *Arch. Rational Mech. Anal.*, vol. **16**, no. 1, pp. 51–78, 1964.

Mindlin, R.D., Influence of Rotatory Inertia and Shear on Flexural Motions of Isotropic, Elastic Plates, *J. Appl. Mech*., vol. **18**, no. 1, pp. 31–38, 2021.

Mondal, S., Sahu, S.A., and Goyal, S., Scattering of Waves at the Interface of Two Distinct Anisotropic Media, *Waves Random Complex Media*, vol. **31**, no. 6, pp. 2407–2426, 2021.

Mühlhaus, H.B. and Aifantis, E., A Variational Principle for Gradient Plasticity, *Int. J. Solids Struct.*, vol. **28**, no. 7, pp. 845–857, 1991.

Needleman, A., Material Rate Dependence and Mesh Sensitivity in Localization Problems, *Comput. Methods Appl. Mech. Eng*., vol. **67**, no. 1, pp. 69–85, 1988.

Nemat-Nasser, S., Lori, M., and Datta, S.K., Micromechanics: Overall Properties of Heterogeneous Materials, *J. Appl. Mech*., vol. **63**, no. 2, pp. 561–561, 1996.

Nguyen, V.P., Lloberas-Valls, O., Stroeven, M., and Sluys, L.J., Computational Homogenization for Multiscale Crack Modeling. Implementational and Computational Aspects, *Int. J. Numer. Methods Eng.*, vol. **89**, no. 2, pp. 192–226, 2012.

Oliveri, F. and Speciale, M., Wave Hierarchies in Continua with Scalar Microstructure in the Plane and Spherical Symmetry, *Comput. Math. Appl*., vol. **55**, no. 2, pp. 285–298, 2008.

Pepe, M., Pingaro, M., Trovalusci, P., Reccia, E., and Leonetti, L., Micromodels for the In-Plane Failure Analysis of Masonry Walls: Limit Analysis, FEM and FEM/DEM Approaches, *Frattura ed Integrita Strutturale*, vol. **14**, no. 51, pp. 504–516, 2019.

Pepe, M., Sangirardi, M., Reccia, E., Pingaro, M., Trovalusci, P., and de Felice, G., Discrete and Continuous Approaches for the Failure Analysis of Masonry Structures Subjected to Settlements, *Front. Built Environ*., vol. **6**, 2020.

Pijaudier-Cabot, G. and Bazant, Z.P., Nonlocal Damage Theory, *J. Eng. Mech*., vol. **113**, no. 10, pp. 1512–1533, 1987.

Pingaro, M., Reccia, E., and Trovalusci, P., Homogenization of Random Porous Materials With Low-Order Virtual Elements, *ASCE-ASME J. Risk Uncert. Eng. Syst. Part B Mech. Eng*., vol. **5**, no. 3, 2019a.

Pingaro, M., Reccia, E., Trovalusci, P., and Masiani, R., Fast Statistical Homogenization Procedure (FSHP) for Particle Random Composites Using Virtual Element Method, *Comput. Mech.*, vol. **64**, no. 1, pp. 197–210, 2019b.

Podio-Guidugli, P. and Vianello, M., Hypertractions and Hyperstresses Convey the Same Mechanical Information, *Continuum Mech. Thermodyn*., vol. **22**, no. 3, pp. 163–176, 2010.

Sadowski, T. and Trovalusci, P., *Multiscale Modeling of Complex Materials: Phenomenological, Theoretical and Computational Aspects*, CISM International Centre for Mechanical Sciences, Vienna: Springer, 2014.

Sadowski, T., Trovalusci, P., Schrefler, B., and de Borst, R., Multi-Scale and Multi-Physics Modelling for Complex Materials, *Meccanica*, vol. **49**, no. 11, pp. 2549–2550, 2014.

Settimi, V., Trovalusci, P., and Rega, G., Dynamical Properties of a Composite Microcracked Bar Based on a Generalized Continuum Formulation, *Continuum Mech. Thermodyn*., vol. **31**, no. 6, pp. 1627–1644, 2019.

Shaat, M., Ghavanloo, E., and Fazelzadeh, S.A., Review on Nonlocal Continuum Mechanics: Physics, Material Applicability, and Mathematics, *Mech. Mater*., vol. **150**, p. 103587, 2020.

Shi, F., Fantuzzi, N., Trovalusci, P., Li, Y., and Wei, Z., The Effects of Dilatancy in Composite Assemblies as Micropolar Continua, *Compos. Struct*., vol. **276**, p. 114500, 2021.

Sluys, L., de Borst, R., and Mu¨ hlhaus, H.B., Wave Propagation, Localization and Dispersion in a Gradient-Dependent Medium, *Int. J. Solids Struct.*, vol. **30**, no. 9, pp. 1153–1171, 1993.

Taliercio, A. and Veber, D., Torsion of Elastic Anisotropic Micropolar Cylindrical Bars, *Eur. J. Mech. A/Solids*, vol. **55**, pp. 45–56, 2016.

Tejchman, J. and Górski, J., Stochastic Fe-Analysis of Shear Localization in 2D Granular Material within a Micro-Polar Hypoplasticity, *Arch. Hydro-Eng. Environ. Mech*., vol. **53**, no. 4, pp. 353–379, 2006.

Trovalusci, P., *Molecular Approaches for Multifield Continua: Origins and Current Developments*, Vienna: Springer, pp. 211–278, 2014.

Trovalusci, P. and Masiani, R., Material Symmetries of Micropolar Continua Equivalent to Lattices, *Int. J. Solids Struct*., vol. **36**, no. 14, pp. 2091–2108, 1999.

Trovalusci, P. and Masiani, R., Non-Linear Micropolar and Classical Continua for Anisotropic Discontinuous Materials, *Int. J. Solids Struct.*, vol. **40**, no. 5, pp. 1281–1297, 2003.

Trovalusci, P., Ostoja-Starzewski, M., De Bellis, M.L., and Murrali, A., Scale-Dependent Homogenization of Random Composites as Micropolar Continua, *Eur. J. Mech. A/Solids*, vol. **49**, pp. 396–407, 2015.

Trovalusci, P. and Pau, A., Derivation of Microstructured Continua from Lattice Systems via Principle of Virtual Works: The Case of Masonry-Like Materials as Micropolar, Second Gradient and Classical Continua, *Acta Mech*., vol. **225**, no. 1, pp. 157–177, 2014.

Tuna, M., Kirca, M., and Trovalusci, P., Deformation of Atomic Models and Their Equivalent Continuum Counterparts Using Eringen's Two-Phase Local/Nonlocal Model, *Mech. Res. Commun*., vol. **97**, pp. 26–32, 2019.

Tuna, M., Leonetti, L., Trovalusci, P., and Kirca, M., 'Explicit'and 'Implicit'non-Local Continuous Descriptions for a Plate with Circular Inclusion in Tension, *Meccanica*, vol. **55**, no. 4, pp. 927–944, 2020.

Tuna, M. and Trovalusci, P., Scale Dependent Continuum Approaches for Discontinuous Assemblies: 'Explicit' and 'Implicit' Non-Local Models, *Mech. Res. Commun.*, vol. **103**, p. 103461, 2020.

Yavari, A. and Marsden, J.E., Covariant Balance Laws in Continua with Microstructure, *Rep. Math. Phys.*, vol. **63**, no. 1, pp. 1–42, 2009.